

Image Quality Assessment for Magnetic Resonance Imaging

Segrey Kastrulyin, Jamil Zakirov, Nicola Pezzotti, and Dmitry V. Dylov

arXiv:2203.07809v1 [eess.IV] 15 Mar 2022

Abstract—Image quality assessment (IQA) algorithms aim to reproduce the human’s perception of the image quality. The growing popularity of image enhancement, generation, and recovery models instigated the development of many methods to assess their performance. However, most IQA solutions are designed to predict image quality in the general domain, with the applicability to specific areas, such as medical imaging, remaining questionable. Moreover, the selection of these IQA metrics for a specific task typically involves intentionally induced distortions, such as manually added noise or artificial blurring; yet, the chosen metrics are then used to judge the output of real-life computer vision models. In this work, we aspire to fill these gaps by carrying out the most extensive IQA evaluation study for Magnetic Resonance Imaging (MRI) to date (14,700 subjective scores). We use outputs of neural network models trained to solve problems relevant to MRI, including image reconstruction in the scan acceleration, motion correction, and denoising. Seven trained radiologists assess these distorted images, with their verdicts then correlated with 35 different image quality metrics (full-reference, no-reference, and distribution-based metrics considered). Our emphasis is on reflecting the radiologist’s perception of the reconstructed images, gauging the most diagnostically influential criteria for the quality of MRI scans: signal-to-noise ratio, contrast-to-noise ratio, and the presence of artifacts.

Index Terms—Image Quality, Deep Learning, Metrics, Reconstruction Quality, Magnetic Resonance Imaging

I. INTRODUCTION

Image quality assessment (IQA) is a research area occupied with constructing accurate computational models to predict the perception of image quality by human subjects, the ultimate consumers of most image processing applications [66].

The growing popularity of image enhancement and image generation algorithms increases the need for a quality assessment of their performance. The demand has led to the abundance of IQA methods emerging over the last decades. The well-known *full-reference* (FR) metrics, such as MSE, PSNR, and SSIM [67], [68], became a de-facto standard in many computer vision applications. The more recent *no-reference*

Sergey Kastrulyin is with Philips Research, Moscow, Russia and Skolkovo Institute of Science and Technology, Moscow, Russia.

Jamil Zakirov is with Skolkovo Institute of Science and Technology, Moscow, Russia.

Nicola Pezzotti is with Philips Research, Eindhoven, and Eindhoven University of Technology, Eindhoven, The Netherlands.

Dmitry V. Dylov is with Skolkovo Institute of Science and Technology, Moscow, Russia. Corresponding author (e-mail:d.dylov@skoltech.ru).

(NR) metrics, such as BRISQUE [42], have also found their use, especially when the ground truth images are absent or hard to access. Yet, another class of *distribution-based* metrics (DB) earned the community’s attention, thanks to the advent of generative adversarial networks (GANs), enabling the quality assessment using distributions of thousands of images instead of gauging them individually. The popular new DB IQA methods include such metrics as Inception Score [54], FID [30], KID [11], MSID [20], and many others. Despite being widely used, the DB metrics were neither included in the recent large scale general domain reviews [4], [41], nor in the medical ones [3].

IQA measures are applied to estimate the quality of image processing algorithms and systems. For example, when several image denoising and restoration algorithms are available to recover images distorted by blur and noise contamination, a perceptual objective IQA could help pick the one that generates the best perceptual image quality after the restoration. To do that reliably, Image Quality Metrics (IQMs) need to show a high correlation with the perceptual estimates of the quality reported by human subjects for a given image processing algorithm. However, IQA algorithms are often *evaluated on non-realistic distortions*, such as added noise or artificial blurring [3], [4], [41]. Such a discrepancy between the synthetic evaluation and the practical use may cause misleading results.

While most metrics are designed to predict image quality in the general domain, Magnetic Resonance Imaging (MRI) provides gray-scale data with the content and style noticeably different from the natural images. Hence, the applicability of the IQMs in the MRI domain must be validated.

Moreover, IQMs trained on natural images attempt to describe the overall perception of the quality of an entire scene. On the contrary, an MRI scan can be perceived as high-quality when specific characteristics, responsible for the scan’s value, are deemed adequate. Those are the characteristics that assist expert radiologists in making their diagnostic decisions, including perceived level of noise (signal-to-noise ratio, SNR), perceived soft tissue contrast (contrast-to-noise ratio, CNR), and the presence of artifacts. These specific quality criteria are, unfortunately, coupled. For example, some denoising algorithms tend to introduce additional blurring (lowering of CNR) in exchange for increased SNR, and some motion correction approaches tend to introduce noticeable artifacts. Therefore, a more detailed evaluation of IQM’s ability to express separate MRI quality criteria is required.

The main contributions of this paper are:

- The most extensive study of IQA in medical imaging, in general, and in MRI, in particular (14,700 subjective scores collected). Unlike previous metric evaluation studies, we avoid artificially added distortions and assess the outputs of *popular image restoration models* instead. The assessment is based on *proposed three criteria* and allows us to make profound conclusions on what modern metrics can capture and when exactly they should be used.
- To the best of our knowledge, we provide the first thorough study of the application of DB metrics for objective IQA of both natural and medical images. We evaluate their performance and show when they give advantage over the common FR and NR metrics. We study the robustness of metrics' performance across these two vastly different domains and show that the best performing IQMs produce valuable results even when the data distribution drastically changes.

II. RELATED WORK

The evaluation of metrics for IQA in the domain of natural images started from the early task-specific works that considered FR methods to characterize color displays and half-toning optimization methods [1].

More recent task-specific studies explored IQA for the images of scanned documents [37] and screen content [72]. Likewise, fused images [65], smartphone photographs [27], remote sensing data [31], and climate patterns [6] demanded the development of targeted IQA approaches. Historically, many of these works have been focusing on the quality degradation caused by the compression algorithms [2], [5], [6], [63], with relatively small datasets appearing publicly for the IQ evaluation. However, the small dataset size and the excessive re-use of the same test sets have led to the promotion of the IQMs poorly generalizable to the unseen distortions.

This was recognized as a major problem, stimulating the emergence of large-scale studies [4], [17]. Among the large-scale evaluations, the majority compared multiple FR metrics, ranging from just a handful [38], [43], [55], [77] to several dozens [4], [47] of IQMs analyzed on popular datasets.

The medical domain stands out from the others by a special sense of what is deemed informative and acceptable in the images [12]. Resulting from years of training and practice, the perception of medical scan quality by adept radiologists relies on a meticulous list of anatomy-specific requirements, on their familiarity with particular imaging hardware, and even on their intuition.

Given the majority of IQMs were not designed for the healthcare domain, some recent works were dedicated to the niche. One small-scale study considered a connection of IQA of natural and medical images via signal-to-noise (SNR) estimation [39]. Others assessed common FR IQMs using non-expert raters [14], [49]. Sufficient for the general audience, these methods proved incapable of reflecting the fine-tuned perception of the radiologists [35].

Expert raters were then engaged in [52] and [3]. The former studied only IQMs from the SSIM family and the latter

assessed 10 FR IQMs, reporting that VIF [56], FSIM [76], and NQM [15] yield the highest correlation with the radiologists' opinions.

On the other hand, Crow *et al.* argue that NR IQA is preferable for assessing medical images because there may be no perfect reference image in the real-world medical imaging [13]. To address this issue, several recent studies also propose new NR IQMs for MRI image quality assessment [32], [45], [46], [57], [60]. Unfortunately, none of these new metrics have an open-source implementation, making verification of the claimed results problematic.

III. IMAGE QUALITY METRICS CONSIDERED

In this work, we evaluate the most widely used and publicly available general-purpose FR, NR, and DB IQMs to find the best algorithms for the quality assessment on arguably the most important MRI-related image-to-image tasks: *scan acceleration*, *motion correction*, and *denoising*. Instead of modeling the disrupted images, we use outputs of trained neural networks and compare them with the clean reference images from the fastMRI dataset.

Our study includes the following 35 metrics: **17 Full-Reference IQMs** (PSNR, SSIM [68], MS-SSIM [70], IW-SSIM [69], VIF [56], GMSD [71], MS-GMSD [74], FSIM [76], VSI [75], MDSI [44], HaarPSI [51], Content and Style Perceptual Scores [33], LPIPS [78], DISTS [16], PieAPP [48], DSS [7]), **3 No-Reference IQMs** (BRISQUE [42], PaQ-2-PiQ [73], MetalQA [79]), and **15 Distribution-Based IQMs** (KID [11], FID [30], GS [36], Inception Score (IS) [54], MSID [20], all implemented with three different feature extractors: Inception Net [21], VGG16, and VGG19 [58]). For brevity of the presentation, we will showcase only the analysis of the best performing four metrics, in the order of their ranking: VSI [75], HaarPSI [51], DISTS [16], and FIDVGG16 [30].

We collect 14,700 ratings from 7 trained radiologists to evaluate the quality of reconstructed images based on three main criteria of quality: perceived level of noise (SNR), perceived soft tissue contrast (CNR), and the presence of artifacts, making this work the most comprehensive study of MRI image quality assessment to date.

IV. MEDICAL EVALUATION

The key goal of this study is to evaluate popular selected IQMs on MRI data. Previous works [3], [52] evaluated the ability of certain IQMs to assess overall quality of data after various types of artificial distortions¹. However, in practice, the overall image quality rating may be insufficient due to its ambiguity: *e.g.*, one could not truly interpret the reasons for poor or good scoring. At the same time, asking the medical experts these general questions may be challenging because of many factors, ranging from the specifics of certain clinical workflows to personal preferences.

In this work, we aspire to solve these problems by proposing the following study. First, we evaluate IQMs with regard to their ability to reflect radiologists' perception of the quality of

¹These artificial distortions, *e.g.*, blurring or JPEG artifacts, are rarely encountered or even impossible in MRI practice.

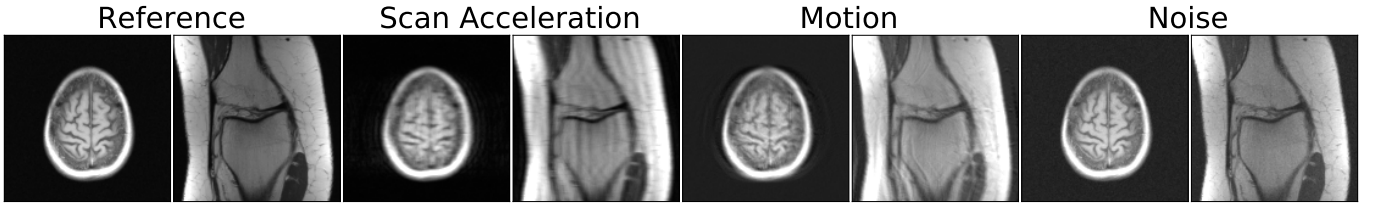


Fig. 1. Distortions introduced to initial artefact-free scans during training and inference. Using the raw k -space data of the reference images, we undersample them with the acceleration factor of 4, impose rigid motion of a moderate amplitude, and introduce mild Gaussian noise. Note how the distortions differ from those in the Natural Images, on which the common IQMs were developed. We adjusted brightness for viewer's convenience.

distorted images, comparing them to the fully-sampled artifact-free ones. We range the metrics based on three IQ criteria that are crucial for making clinical decisions: perceived level of noise (SNR), perceived level of contrast (CNR), and the presence of artifacts. Second, instead of corrupting images with artificial perturbations, for the first time in the community, we validate these metrics using the actual outputs of deep learning networks trained to solve common MR-related tasks. As such, the artifacts originate from the imperfect solutions to the common real-world problems of motion correction, scan acceleration, and denoising.

A group of trained radiologists rated the quality of distorted images compared to the clean reference images on a scale from 1 to 4 for the three IQ criteria. The aggregated evaluation results were compared with the values of selected IQA algorithms to identify top performers – the metrics that have the highest correlation scores with the radiologists' ratings.

A. Image Library Generation

As a data source, we use the largest publicly available repository of raw multi-coil MRI k -space data – the FastMRI dataset, containing the knee and the brain scans [22], [23]. The knee subset of FastMRI contains 1,500 fully sampled MRIs acquired with a 2D protocol in the coronal direction with 15 channel knee coil array on 3 and 1.5 Tesla Siemens MRI machines. The data consists of approximately equal number of scans acquired using the proton density weighting with (PDFS) and without (PD) fat suppression pulse sequences with the pixel size of $0.5 \text{ mm} \times 0.5 \text{ mm}$ and the slice sickness of 3 mm.

The knee subset is divided into 4 categories: train (973 volumes), validation (199 volumes), test (118 volumes), and challenge (104 volumes). Only the multi-coil scans were selected for this study, omitting the single-coil data.

The brain subset includes 6,970 1.5 and 3 Tesla scans collected on Siemens machines using T1, T1 post-contrast, T2, and FLAIR acquisitions. Unlike the knee subset, this data are of a wide variety of reconstruction matrix sizes. For the purpose of de-identification, authors of the dataset limited the data to only 2D axial images, and replaced k -space slices $\gtrsim 5 \text{ mm}$ below the orbital rim with zero matrices. The brain subset is divided into 6 categories: train (4,469 volumes), validation (1,378 volumes), test 4 \times (281 volumes), test 8 \times (277 volumes), challenge 4 \times (303 volumes), and challenge 8 \times (262 volumes).

Starting with the clean knee and brain data, we first generate images corrupted with three types of distortions: scan acceleration, motion, and noise. The examples of the distorted images are presented in Fig. 1.

1) Scan Acceleration: Scan-acceleration data are generated from the ground truth images by undersampling the k -space data. To train the model, we selected only T1 weighted scans (T1, T1-PRE and T1-POST) from the train category of the FastMRI brain data. The same subset of data was used for training of motion correction and denoising models. The k -space data were subsampled using a Cartesian mask, where k -space lines are set to zero in the phase encoding direction. The sampled lines are selected randomly, with the total sampling density depending on the chosen acceleration rate. Following the data generation process from the FastMRI challenge [22], all masks are fully sampled in the central area of k -space (the low frequencies). For the 4 \times accelerated scans, this corresponds to 8%, and for the 8 \times acceleration, it equals to 4%. Besides making the reconstruction problem easier to solve, such lines allow computing the low-pass filtered versions of the images for assessing the coil sensitivity maps.

To compensate for the undersampling, we used the 2019 FastMRI challenge winner Adaptive-CS-Net model [24]. Based on the Iterative Shrinkage-Thresholding Algorithm (ISTA) [9], this model consists of several trainable convolutional multi-scale transform blocks between which several prior knowledge-based computations are implemented. For scalability reasons and without substantially impacting the reconstruction results, in this study we trained a simplified and light-weight version of the Adaptive-CS-Net model using PyTorch [19]. The resulting model consists of only 10 trainable blocks and 267k parameters, with soft data consistency being the only prior applied between the reconstruction blocks. We trained the model using RMSprop optimizer [61] using step-wise learning rate decay of 10^{-4} to reconstruct the data for various accelerations (from 2 \times to 8 \times). Two models trained for 2 and 4 epochs on brain multi-coil train data were selected for further data generation.

2) Motion Correction: The in-plane motion artifacts, including rigid translation and rotation, were introduced into the Fourier-transformed data following the procedure described in [59]. For each input image, the assumed echo-train length of the turbo spin-echo readout was chosen randomly in the 8–32 range. Similarly, the assumed extent of zero-padding in k -space was chosen randomly in the range of 0–100. The motion trajectories (translation/rotation vectors as a function of

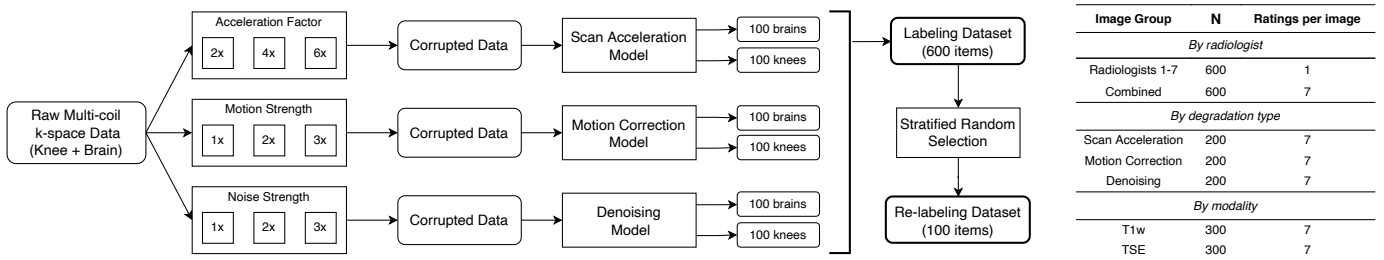


Fig. 2. Formation of Labeling and Re-labeling datasets for annotation (left) and the content of each group of images for the medical evaluation and labeling by radiologists in the Labeling dataset (right). Starting from the clean validation data, we first generate corrupted data with the acceleration artefacts, the motion artefacts, and the Gaussian noise. Then, we reconstruct the corrupted data using trained neural network models and randomly select scans to form labeling and re-labeling pairs for the experts to grade.

scan time) were generated randomly to simulate the realistic artifacts. In this study we utilized the protocol for “sudden motion” simulation. Here, the subject is assumed to lie still for a large part of the examination, until a swift translation or rotation of the head occurs. The time point of the sudden motion was taken randomly as a fraction of the total scan time in the range of one-third to seven-eighths.

To compensate for the motion artefacts of various extent, we trained the original U-Net model [53]. The model received the motion corrupted data as the input and learned to predict the motion artefacts in a residual manner, *i.e.*, the output of the model was a predicted image of motion in the input data. The model was trained to minimise L1 loss between the ground-truth and the predicted residual with Adam [34] optimizer using the step-wise learning rate decay of 10^{-4} . Preserving the same nature of artifacts, we trained our models for a range of amplification factors (from 1 to 3) to account for the varying levels of appearance of the motion artefacts that can be met in practice. Two models trained using PyTorch [19] for 2 and 4 epochs on brain multi-coil train data were selected for further data generation.

3) Denoising: Denoising data are generated from the ground truth images by adding the Gaussian noise to the magnitude images. The parameters of the noise distribution for each volume are drawn from the last slice of this volume. After that, the Gaussian noise with the estimated distribution parameters is scaled by an amplification factor and added to all images of the volume. We used amplification factor of 2 for training and amplification factors of 1, 2, and 3 for test data generation.

To compute denoised images, we trained two DnCNN models [18] for 2 and 4 epochs on brain multi-coil train data using PyTorch [19], RMSprop optimizer [61], and step-wise learning rate decay of 10^{-4} .

4) Final Dataset for Labeling: We started the formation of the labeling dataset from the clean volumes from the validation subsets of brain and knee FastMRI datasets; hence, these scans were not used to train the artefacts correction models. In total, both validation subsets contain 1,577 volumes, resulting in 28,977 images: 199 knee volumes with 7,135 slices and 1,378 brain volumes with 21,842 slices. In each brain volume, the lower 2 and top 3 slices were discarded to restrict the analysis to clinically relevant parts of the scan. In each knee volume, the first 3 slices were discarded for the same reason. To limit

the number of data points and decrease the overall variability of data types, we selected only T1-weighted (T1, T1-PRE and T1-POST) brain volumes and proton-density weighted without fat suppression (PD) knee volumes.

The data generation pipeline is summarized in Fig. 2.

Using the selected subset of clean validation data, we simulated images for the reconstruction:

- For the scan acceleration task, we simulated acceleration artefacts for undersampling rates of 2x, 4x, and 6x, following the data generation process from the FastMRI challenge;
- For the motion correction task, we simulated motion artefacts of three different strengths using the rigid motion simulation framework described above;
- For the denoising task, we simulated Gaussian noise with amplification factors of 1, 2 and 3 using the noise generation procedure described above.

After that, all generated corrupted data were reconstructed using the reconstruction models trained for the corresponding tasks. Note that we deliberately generated a fraction of data with parameters different from the ones used to train the reconstruction models. We found this approach yields various levels of artefacts typically appearing after the reconstruction process.

From the large pool of reconstructed images, we select 100 pairs of images (clean - reconstructed) for each task (scan acceleration, motion correction, denoising) and each anatomy (knee, brain), evenly distributing the data to represent each reconstruction parameter (*e.g.*, the acceleration rate for the scan acceleration task). This strategy results in the labeling dataset of 600 pairs of images in total (3 tasks \times 2 anatomies).

To reach the goal labeling dataset size, we utilized the following data selection procedure:

- 1) Compute values of IQMs for all reconstructed images (for NR IQMs) or image pairs (for FR IQMs);
- 2) Normalize each IQM value to $[0, 1]$;
- 3) Compute variance between IQM values for all items;
- 4) Sort all items by the value of variance;
- 5) Select 25% of data for each task-anatomy combination from the data items with the highest variance, assuming that items with the biggest disagreement between IQMs are the most informative;
- 6) Select the rest 75% of data pseudo-randomly (preserve distribution of reconstruction parameters) to avoid intro-

ducing any bias from the variance computation.

Lastly, we deliberately duplicated 100 of the 600 prepared items for the purpose of verification of radiologists' self-consistency, resulting in 700 image pairs to be labelled by each radiologist.

B. Experiment Setup

Within the paradigm of the model observer framework [8], the quality of a medical image can be defined as how well a clinical task (*e.g.*, diagnostics) can be performed on it [29]. This means that the perfect MRI IQM would be some task-based score, such as the diagnostic accuracy. However, such a metric is difficult to implement due to a great diversity of diagnostic outcomes that radiologists deal with in practice. Because of that, the convention is to use a *subjective estimation* of the overall diagnostic value instead [3].

However, we argue that a single score is not sufficient to reflect the abundance of anatomies, pathologies, and artefactual cases that the radiologists work with. Instead, we propose to subdivide the score of the overall diagnostic quality into three main criteria that can be important for a clinical practitioner to make their decision: i) perceived level of noise, ii) perceived level of soft-tissue contrast, and iii) presence of artefacts.

1) Subjective Evaluation: Seven trained radiologists took part in this study. The participants were asked to score pairs of reconstructed-reference images using three main IQ criteria. For each image pair and each criterion, radiologists scored the perceived diagnostic quality of the reconstructed image compared to the ground-truth using a four-point scale: not acceptable (1), weakly acceptable (2), rather acceptable (3), and fully acceptable (4). The four-point scale was selected over the five-point Likert scale, previously used in [3].

Each participant performed the labelling individually using a dedicated instance of the Label Studio [62] software accessible via a web interface. The experts were asked to make all judgments about the image quality with regard to a particular diagnostic task that they would normally perform in their practice (*e.g.*, the ability to discriminate relevant tissues, the confidence in using the image to detect a pathology, *etc.*). The interface provided additional functionality of scaling (zooming) the images to closer mimic the real-life workflow. The pairs of images were displayed in a random order until all pairs were labelled. Participants had an opportunity to re-label the pairs they have already scored at any point until the experiment is finished.

During the main part of the experiment, each participant labelled 600 pairs of images based on the 3 quality criteria, resulting in 4,200 annotated pairs and 12,600 labels in total. The results of the main labelling session were used for further evaluation of the IQMs. After finishing the main part of the experiment, the participants were asked to additionally label 100 randomly selected pairs from the same dataset, yielding additional 2,100 labels. The results of this additional re-labelling were used to evaluate the self-consistency of each annotator.

2) Metrics Computation: Unlike FR and NR IQMs, designed to compute an image-wise distance, the DB metrics compare distributions of *sets* of images. This makes them less practical for traditional IQA, the goal of which is to compute a score for a given image pair. Moreover, the need to have sets of images hinders the vote-based evaluation via the mean subjective opinion scores.

To address these problems, we adopt a different way of computing the DB IQMs. Instead of extracting features from the whole images, we crop them into overlapping tiles of size 96×96 with $stride = 32$. This pre-processing allows us to treat each pair of images as a pair of distributions of tiles, enabling further comparison. The other stages of computing the DB IQMs are kept intact.

C. Data Analysis

Here, we adapt the analysis of the scoring data proposed in [55] to the multiple IQ criteria. The voting scores for each scoring criteria are not analyzed in their raw format. Instead, they are converted to z-scores (averaged and re-scaled from 0 to 100 for each radiologist to account for their different scoring):

$$z_{nmk} = (D_{nmk} - \mu_{mk}) / \sigma_{mk}, \quad (1)$$

where μ_{mk} and σ_{mk} are the mean and the standard deviation of the difference scores of the m^{th} radiologist on the k^{th} scoring criteria, and D_{nmk} are the difference scores for n^{th} degraded image defined as follows:

$$D_{nmk} = s_{mk,\text{ref}} - s_{nmk}. \quad (2)$$

In Eq. (2), $s_{mk,\text{ref}}$ is the raw score of the m^{th} radiologist on the k^{th} scoring criteria for the reference image corresponding to the n^{th} degraded image, and s_{nmk} is the raw score of the m^{th} radiologist on the n^{th} degraded image on the k^{th} scoring criteria. Note that in this study, the radiologists were asked to perform pair-wise comparison between degraded and reference images. Hence, it is possible to treat the raw labelling scores as the difference scores D_{nmk} .

After standardizing the expert votes by Eq. (1), their correlation statistics with each IQM were computed in the form of SRCC and KRCC coefficients. We use SRCC as the main measure of an IQM performance, due to the non-linear relationship between the subjective and the objective scores².

The sizes of each batch of data are described in Fig. 2 (right).

A non-linear regression was performed on the IQM scores according to the quality Q to fit the subjective votes:

$$Q(x) = \beta_1 \left(\frac{1}{2} - \frac{1}{1 + \exp(\beta_2(x - \beta_3))} \right) + \beta_4 x + \beta_5, \quad (3)$$

where x are the original IQM scores and β_1, \dots, β_5 are the fitting coefficients.

²The non-linear relationship is evident in Fig. 4 below.

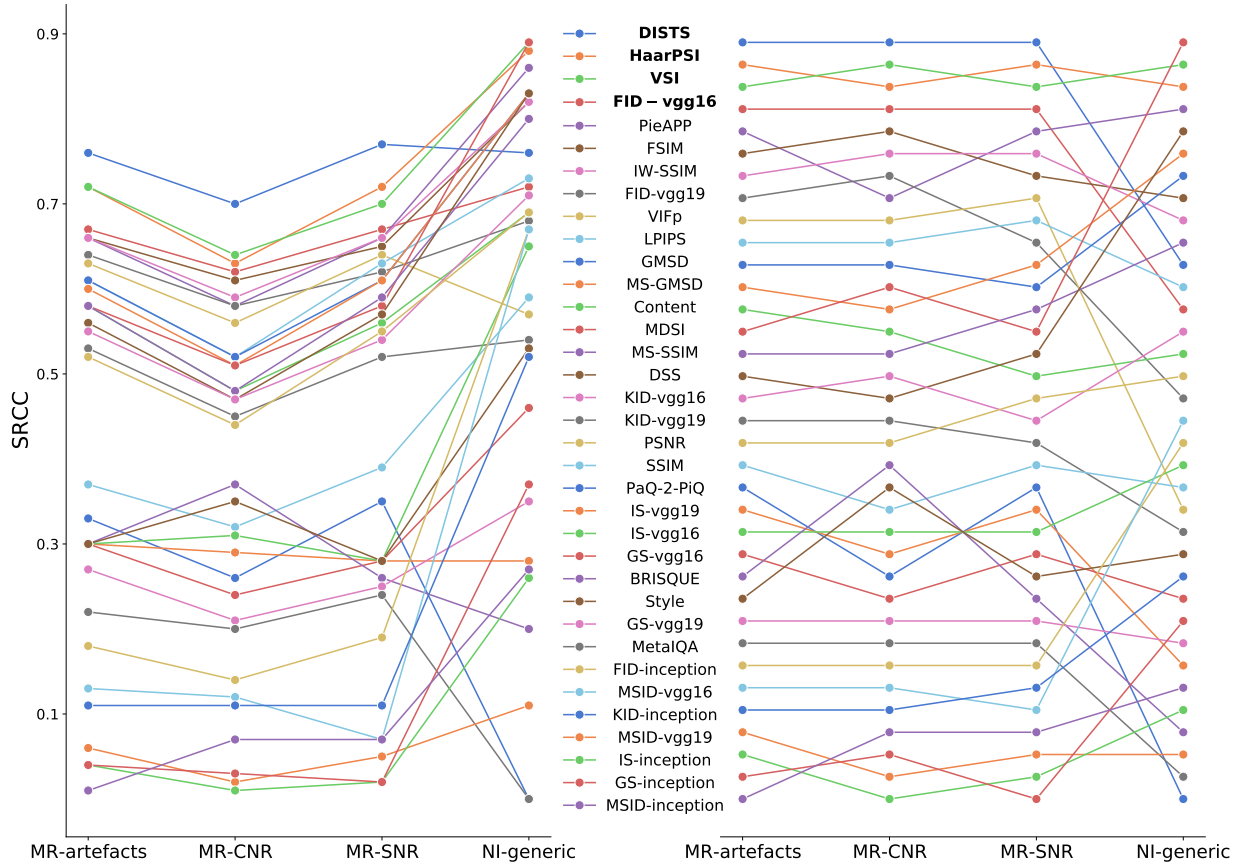


Fig. 3. Performance of IQMs on different MRI tasks and on Natural Images (NI), compared by their correlation with the expert votes (SRCC values, left) and sorted top-to-bottom by their rank (right). The ordering reflects the performance on the MRI data only. The same color-coding is used in both plots. *NI-generic* scores are the average between TID2013 [25] and KADID-10k [40] datasets. Note higher correlation of IQMs on NI and poor translation of ranking to MRI domain. Refer to data in Table I for numerical values.

V. RESULTS

Figs. 3 and 4 and Table I summarize the correlation study between the radiologists' scores and the IQM values for the three proposed evaluation criteria. Also shown are the results for the natural image domain. Top 4 performers in each category are marked in bold. The best and the worst examples of the reconstructions, as judged by different metrics, are presented in Fig. 5, and the aggregate scores for the top-performing metrics in each application in Fig. 6.

VI. DISCUSSION

The visual inspection of the outputs of the models in Fig. 5 makes it evident how the top metrics are superior in reflecting the actual reconstruction quality over the conventional PSNR and SSIM. The latter are known to misjudge shifts of brightness or a blur, indicating high quality for the bad images, whereas the more advanced FR and DB IQMs correlate with the visual perception and the subjective scores ably. Henceforth, out of the 35 metrics considered, we only discuss the best ones, according to their rank in the correlation study (VSI, HaarPSI, DISTs, FID_{VGG16}) and the widely used PSNR and SSIM.

As the key observation in the first systematic study of the DB metrics, we affirm that the choice of the feature extractor

plays a crucial role. In particular, the correlation scores show that the Inception-based features are almost always worse than those from VGG16 (except for the MSID metric). Moreover, we see that, despite having been designed for the evaluation of *realism* of generative models data, FID shows competitive SRCC scores, thus, becoming a new recommended metric for the MRI image assessment tasks.

The non-linear relationship between the subjective and the objective scores, seen in Fig. 4, portrays intricate behavior with evident dependence on the anatomy and the target task, as well as a clear clustering of the points, instrumental for selecting a proper metric in a particular application. Notable are the generally lower IQM correlation scores when the difficulty of the reconstruction routine increases (compare trends in the scan acceleration data to those in the more complex denoising and the motion correction models). Also, the evaluation values for the knee reconstruction are generically lower, which could be caused by the greater variety of anatomical structures present in the knee data, as well as the more strict pertinent medical evaluation criteria [35].

Fig. 6 aggregates the outcomes per each task, anatomy, and evaluation criteria studied in our work, with the relation between the subjective and the objective scores highlighting the differences in the average performance of the top metrics. Notably, these selected IQMs have the highest correlation

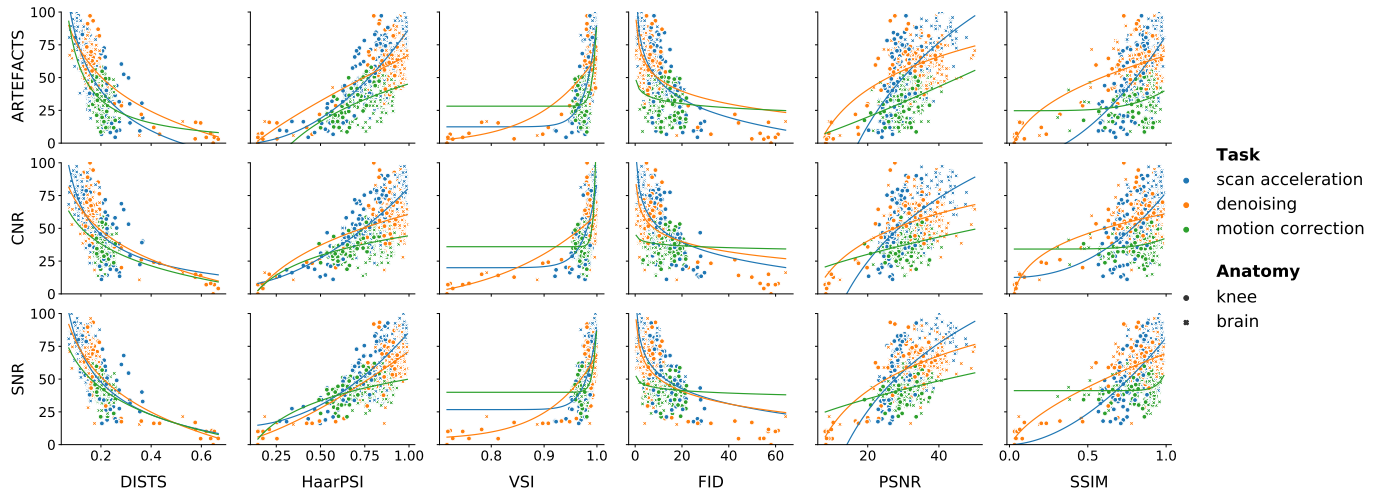


Fig. 4. Relationship between processed subjective scores and IQM values for 3 evaluation criteria, 3 target tasks, and 2 anatomies (600 annotated image pairs in total). The solid lines are fits, plotted using the non-linear regression (3) on the subsets of images split by the tasks. The top 4 metrics (along with PSNR and SSIM, as the most commonplace) are shown in the decreasing order left to right, using SRCC to gauge the performance.

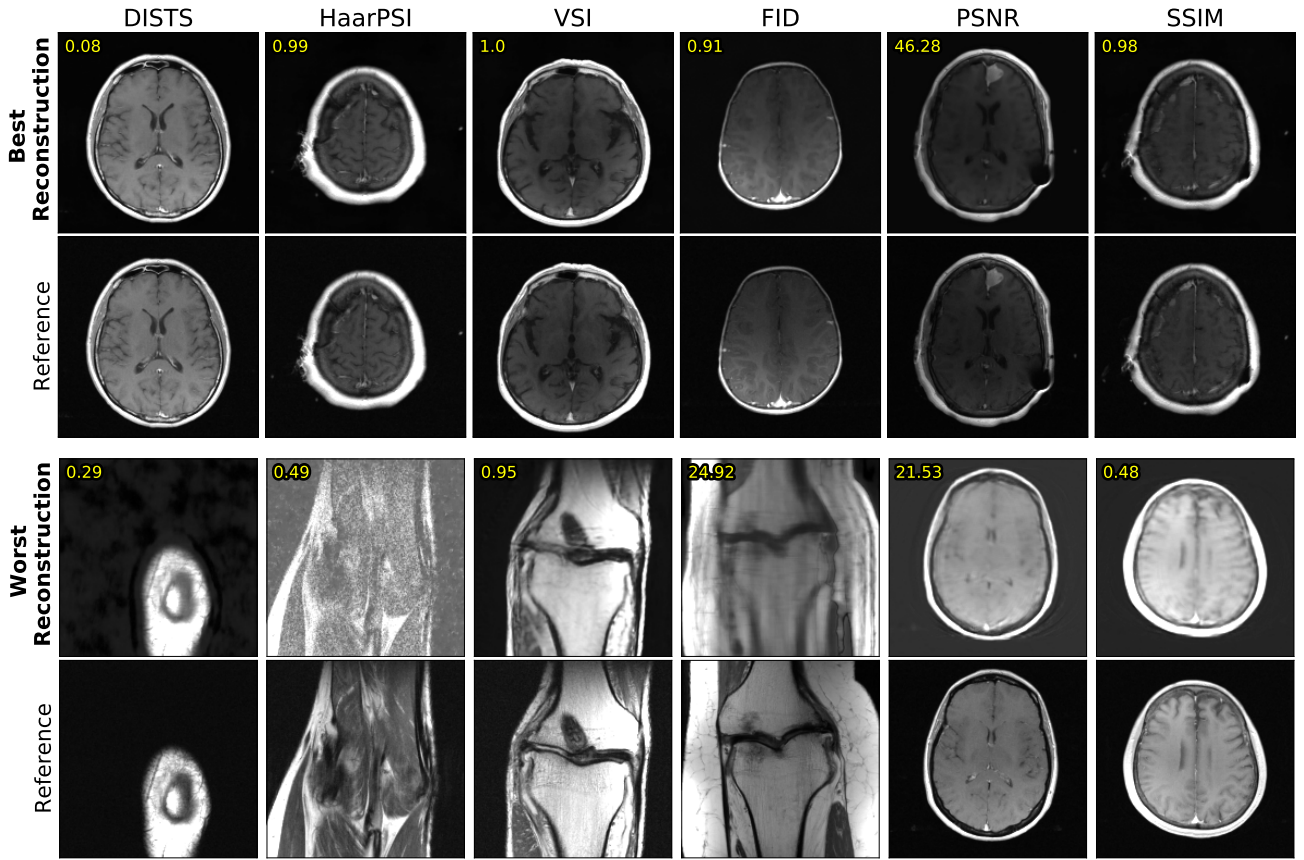


Fig. 5. The best and the worst reconstruction-reference pairs according to different metrics (their values are shown in yellow). Note how the top 4 metrics (first four columns) reflect the actual reconstruction quality better than PSNR and SSIM (which are prone to misjudging a simple shift of brightness or a blur). The brightness is adjusted for viewer's convenience.

with expert judgment in the scan acceleration task. However, all metrics equally struggle reflecting the opinion of the radiologists in denoising and, sometimes, in motion correction tasks, especially on brain data. We also observe that some metrics perform consistently in terms of all three evaluation criteria and all tasks for given anatomy. For instance, GMSD

and DISTs, despite not being of the highest SRCC rank overall, still show consistently high correlation scores on knee data, which proffers both of them as universal choices for the IQA in orthopedic applications. On the other hand, HaarPSI consistently rates the highest for both anatomies in the scan acceleration task, an instrumental fact to know when a single

TABLE I

SRCC VALUES OF ALL 35 METRICS ON NATURAL AND MRI DATA.
TOP 4 PERFORMERS IN ALL CATEGORIES ARE MARKED IN BOLD.
* DENOTES VALUES TAKEN DIRECTLY FROM [28]

	Natural Images		MRI Data		
	TID2013	KADID-10k	Artefacts	CNR	SNR
PSNR	0.69	0.68	0.52	0.44	0.55
SSIM [68]	0.55	0.63	0.37	0.32	0.39
MS-SSIM [70]	0.80	0.80	0.58	0.48	0.59
IW-SSIM [69]	0.78	0.85	0.66	0.59	0.66
VIFp [56]	0.46	0.67	0.63	0.56	0.64
GMSD [71]	0.80	0.85	0.61	0.52	0.61
MS-GMSD [74]	0.81	0.85	0.60	0.51	0.61
FSIM [76]	0.80	0.84	0.66	0.61	0.65
VSI [75]	0.89	0.88	0.72	0.64	0.70
MDSI [44]	0.89	0.89	0.58	0.51	0.58
HaarPSI [51]	0.87	0.88	0.72	0.63	0.72
ContentVGG16 [33]	0.67	0.71	0.58	0.48	0.56
StyleVGG16 [33]	0.50	0.56	0.30	0.35	0.28
LPIPS _{VGG16} [78]	0.67	0.78	0.61	0.52	0.63
DISTS [16]	0.71	0.81	0.76	0.70	0.77
PieAPP [48]	0.84	0.87	0.66	0.58	0.66
DSS [7]	0.79	0.86	0.56	0.47	0.57
No-reference metrics					
BRISQUE [42]	0.20	0.20	0.30	0.37	0.26
PaQ-2-PIQ [73]	0.86*	0.84*	0.33	0.26	0.35
MetaIQA [79]	0.86*	0.76*	0.22	0.20	0.24
Distribution-based metrics					
KID _{InceptionV3} [11]	0.42	0.63	0.11	0.11	0.11
FID _{InceptionV3} [30]	0.67	0.66	0.18	0.14	0.19
GS _{InceptionV3} [36]	0.37	0.37	0.04	0.03	0.02
IS _{InceptionV3} [54]	0.26	0.25	0.04	0.01	0.02
MSID _{InceptionV3} [20]	0.21	0.32	0.01	0.07	0.07
KID _{VGG16} [11]	0.70	0.71	0.55	0.47	0.54
FID _{VGG16} [30]	0.67	0.66	0.67	0.62	0.67
GS _{VGG16} [36]	0.47	0.45	0.30	0.24	0.28
IS _{VGG16} [54]	0.64	0.65	0.30	0.31	0.28
MSID _{VGG16} [20]	0.69	0.64	0.13	0.12	0.07
KID _{VGG19} [11]	0.54	0.59	0.53	0.45	0.52
FID _{VGG19} [30]	0.68	0.75	0.64	0.58	0.62
GS _{VGG19} [36]	0.35	0.41	0.27	0.21	0.25
IS _{VGG19} [54]	0.28	0.33	0.30	0.29	0.28
MSID _{VGG19} [20]	0.11	0.13	0.06	0.02	0.05

machine is used to scan various body parts or when the pertinent cross-anatomy inference [10] is performed.

A. Natural vs. MRI Images

A frequent IQA-related question is how generalizable are the performance benchmarks across different datasets and image domains. To study that, we analyzed the applicability of all 35 IQMs considered herein both in the MRI and the natural image (NI) domains (Table I). For the latter, the popular TID2013 [25] and KADID-10k [40] datasets of NIs were used. Fig. 3 illustrates the effect of the shift between the NI and the MRI domains, featuring an expected drop of the correlation values for most metrics³. However, the domain shift affects the ranks of the IQMs differently. Some top NI metrics, such as MDSI and MS-GMSD, naturally take lower standings in

³Not surprising, given these IQMs were designed for NI in the first place.

the MRI domain; however, others, such as HaarPSI and VSI, remain well-correlated with the radiologists' perception of quality. Further examples of IQMs robust to the domain shift are DISTS and FID_{VGG16}, although they are marginally below HaarPSI and VSI in the ranking.

B. Labeling Discrepancies and Self-Consistency Study

Another IQA-related question encountered in survey-based studies is the trustworthiness of the votes themselves. Given that only reputable radiologists were engaged in our labeling routine, we have no grounds for doubting their annotations as far as the domain knowledge is concerned. Therefore, feasible discrepancies among their votes can be assumed to originate either from such factors as the study design, its duration, and fatigue, or from a previous experience which sometimes forms a *a posteriori* intuition and, allegedly, influences the experts to make decisions different from the others.

While the latter is too subjective and difficult to regulate, the former could be controlled. We put effort to simplify the user experience and allowed the radiologists to approach the labeling assignment in batches at their own pace. The average lead time spent labeling a pair of images⁴, an arguable indicator of the scrupulousness of an annotator, is plotted in Fig. 7, where we also summarize the results of the self-consistency study. The study reports Weighted Cohen's Kappa scores, computed between the votes provided in the main and in the additional re-labeling experiments on the same data. Interestingly, there is no significant correlation between self-consistency and the labeling time, placing other factors mentioned above, such as individual experience, at the forefront.

In Fig. 7, the Weighted Cohen's Kappa values correspond to *moderate to substantial* consistency of scoring (according

⁴We discarded 5% of the shortest and the longest lead times to account for erroneous clicks and breaks between the labeling sessions.

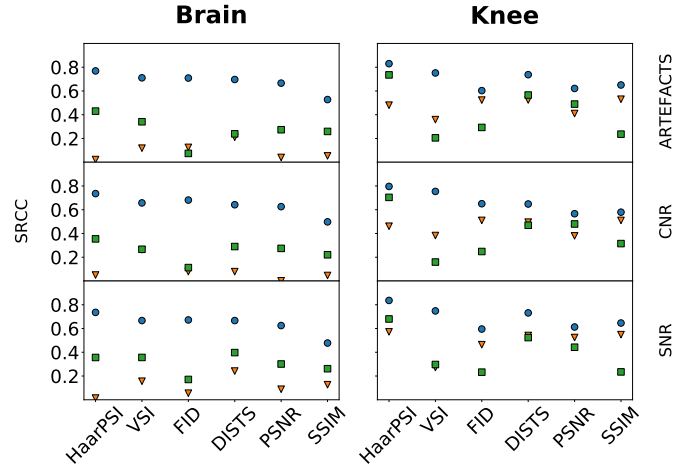


Fig. 6. Aggregate relationship between the objective and the subjective scores for 3 evaluation criteria (rows), 2 anatomies (columns), and 3 tasks: scan acceleration (●), denoising (▽), and motion correction (■). The IQMs are ordered by decreasing average SRCC for the artefacts criterion on the brain data. This order is kept throughout all results for consistency. Note the tendency of the metrics to perform poorly in some task-anatomy combinations, e.g., in denoising the brain data.

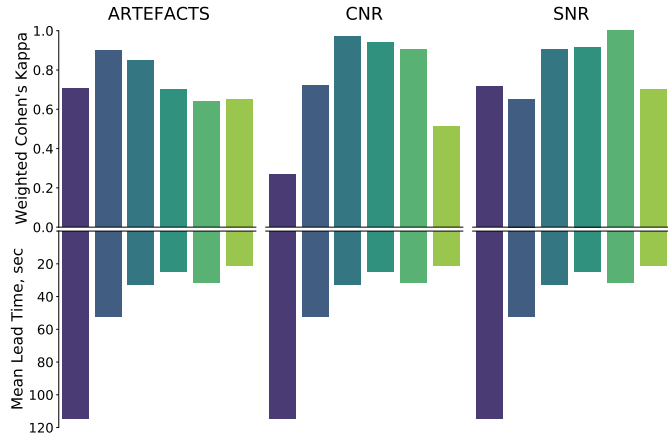


Fig. 7. Correlation between the subjective scores in labelling and re-labelling sessions on the same data, with each column/color corresponding to an individual radiologist. This plot shows scoring self-consistency of the experts and the average time spent labelling one pair of images. Apparently, the time spent on labelling is not the major factor affecting the self-consistency of experienced radiologists.

to [64]). Given the sufficiently trustworthy labeling, the spread of the correlation scores for the modern IQA metrics in Fig. 6, and the non-trivial correlation patterns in Fig. 4, one can conclude that *the optimal MRI metric is yet to be devised*.

Besides a blunt umbrella metric aggregating the top-performing predictions (*e.g.*, those of VSI, HaarPSI, DISTs, and FID_{VGG16}), the future effort should be dedicated to additional forays into modeling *MRI-specific perception* of the radiologists and to *interpreting* their assessment using formalized rules taken from the medical textbooks. Such interpretable metrics will be especially in demand, given the recent appearance of the MRI sampling approaches aimed towards optimizing downstream tasks [50], including the recently annotated FastMRI dataset [26]. Another line of future work could be ‘borrowed’ from the NI domain, where the abundance of data has led to the emergence of several NR IQMs. Although, in our study, all such metrics (classic BRISQUE [42] and the more recent PaQ-2-PiQ [73] and MetaIQA [79]) showed equally mediocre performance compared to the other IQMs, we believe their value in the MRI domain is bound to improve with the growth of available data.

VII. CONCLUSION

This manuscript reports the most extensive study of the image quality metrics for Magnetic Resonance Imaging to date, evaluating 35 modern metrics and using 14,700 subjective votes from experienced radiologists. The top performers – HaarPSI, VSI, DISTs, and FID_{VGG16} – are found to be efficient across three proposed quality criteria, for all considered anatomies and the target tasks.

ACKNOWLEDGMENTS

We acknowledge the effort of radiologists from the Philips Clinical Application Team (PD CEER) for their help with data labeling and thank the supporters of our GitHub project⁵, where each metric was independently implemented and tested.

⁵<https://github.com/photosynthesis-team/piq/>

REFERENCES

- [1] A. J. Ahumada. Computational image quality metrics: A review. *SID Digest*, 24(January 1993):305–308, 1993.
- [2] E. Allen, S. Triantaphillidou, and RE Jacobson. Image quality of jpeg vs jpeg 2000 image compression schemes, part 1: Psychophysical measurements. *IS&T J. Imaging Sci. Technol.*, 51(3):248–258, 2007.
- [3] Allister Mason *et. al.*; Comparison of Objective Image Quality Metrics to Expert Radiologists’ Scoring of Diagnostic Quality of MR Images. *IEEE Transactions on Medical Imaging*, 39(4):1064–1072, 2020.
- [4] Shahrukh Athar and Zhou Wang. A comprehensive performance evaluation of image quality assessment algorithms. *IEEE Access*, 7:140030–140070, 2019.
- [5] Niranjan Avadhanam and V Ralph Algazi. Evaluation of a human-vision-system-based image fidelity metric for image compression. In *Applications of Digital Image Processing XXII*, volume 3808, pages 569–579. International Society for Optics and Photonics, 1999.
- [6] A. H. Baker, D. M. Hammerling, and T. L. Turton. Evaluating image quality measures to assess the impact of lossy data compression applied to climate simulation data. *CGF*, 38(3):517–528, 2019.
- [7] Amnon Balanov, Arik Schwartz, Yair Moshe, and Nimrod Peleg. Image quality assessment based on dct subband similarity. In *2015 IEEE ICIP*, pages 2105–2109, 2015.
- [8] H H Barrett, J Yao, J P Rolland, and K J Myers. Model observers for assessment of image quality. *Proceedings of the National Academy of Sciences*, 90(21):9758–9765, 1993.
- [9] Amir Beck and Marc Teboulle. A fast iterative shrinkage-thresholding algorithm for linear inverse problems. *SIAM journal on imaging sciences*, 2(1):183–202, 2009.
- [10] A. Belov, J. Stadelmann, S. Kastryulin, and D. V. Dylov. Towards Ultrafast MRI via Extreme k-Space Undersampling and Superresolution. In *MICCAI 2021*, pages 254–264, Cham, 2021.
- [11] M. Binkowski, D. J. Sutherland, M. Arbel, and A. Gretton. Demystifying MMD gans. In *ICLR 2018*, 2018.
- [12] Christine Cavarro-Menard, Lu Zhang, and Patrick Le Callet. Diagnostic quality assessment of medical images: Challenges and trends. *EUVIP2010*, pages 277–284, 2010.
- [13] L. S. Chow and R. Paramesran. Review of medical image quality assessment. *Biomed. Signal Process. Control.*, 27:145–154, 2016.
- [14] L. S. Chow, H. Rajagopal, and R. Paramesran. Correlation between subjective and objective assessment of magnetic resonance (MR) images. *Magnetic Resonance Imaging*, 34(6):820–831, 2016.
- [15] Niranjan Damera-Venkata, Thomas D. Kite, Wilson S. Geisler, Brian L. Evans, and Alan C. Bovik. Image quality assessment based on a degradation model. *IEEE TMI*, 9(4):636–650, 2000.
- [16] Keyan Ding, Kede Ma, Shiqi Wang, and Eero P Simoncelli. Image quality assessment: Unifying structure and texture similarity. *arXiv:2004.07728*, 2020.
- [17] Keyan Ding, Kede Ma, Shiqi Wang, and Eero P. Simoncelli. Comparison of full-reference image quality models for optimization of image processing systems. *Int. J. Comput. Vis.*, 129(4):1258–1281, 2021.
- [18] Chao Dong, Chen Change Loy, Kaiming He, and Xiaoou Tang. Image super-resolution using deep convolutional networks. *IEEE transactions on pattern analysis and machine intelligence*, 38(2):295–307, 2015.
- [19] Adam Paszke *et. al.* Pytorch: An imperative style, high-performance deep learning library. In *Advances in Neural Information Processing Systems 32*, pages 8024–8035. 2019.
- [20] Anton Tsitsulin *et. al.* The shape of data: Intrinsic distance for data distributions. In *ICLR 2020: Proceedings of the International Conference on Learning Representations*, 2020.
- [21] Christian Szegedy *et. al.* Going deeper with convolutions. In *Proceedings of the IEEE CVPR*, pages 1–9, 2015.
- [22] Florian Knoll *et. al.* fastmri: A publicly available raw k-space and dicom dataset of knee images for accelerated mr image reconstruction using machine learning. *Radiology: Artificial Intelligence*, 2(1):e190007, 2020. PMID: 32076662.
- [23] Jure Zbontar *et. al.* fastmri: An open dataset and benchmarks for accelerated mri. *arXiv:1811.08839*, 2019.
- [24] Nicola Pezzotti *et. al.* An adaptive intelligence algorithm for undersampled knee mri reconstruction. *IEEE Access*, 8:204825–204838, 2020.
- [25] Nikolay Ponomarenko *et. al.* Image database tid2013: Peculiarities, results and perspectives. *Sig proc: Image com*, 30:57–77, 2015.
- [26] R. Zhao *et. al.* fastmri+: Clinical pathology annotations for knee and brain fully sampled multi-coil mri data. *arXiv:2109.03812*, 2021.
- [27] Y. Fang, H. Zhu, Y. Zeng, K. Ma, and Z. Wang. Perceptual quality assessment of smartphone photography. In *Proceedings of the IEEE Computer Society Conference on CVPR*, pages 3674–3683, 2020.

[28] S. Alireza Golestaneh, Saba Dadsetan, and Kris M. Kitani. No-reference image quality assessment via transformers, relative ranking, and self-consistency. *CoRR*, abs/2108.06858, 2021.

[29] Xin He and Subok Park. Model Observers in Medical Imaging Research. *Theranostics*, 3(10):774, 2013.

[30] M. Heusel, H. Ramsauer, T. Unterthiner, B. Nessler, and S. Hochreiter. Gans trained by a two time-scale update rule converge to a local nash equilibrium. In *Adv Neural Inform Process Syst*, pages 6626–6637, 2017.

[31] O. Ieremeiev, V. Lukin, K. Okarma, and K. Egiazarian. Full-Reference Quality Metric Based on Neural Network to Assess the Visual Quality of Remote Sensing Images. *Remote Sensing 2020, Vol. 12, Page 2349*, 12(15):2349, 2020.

[32] J. Jang, K. Bang, H. Jang, and D. Hwang. Quality evaluation of no-reference MR images using multidirectional filters and image statistics. *Magnetic Resonance in Medicine*, 80(3):914–924, sep 2018.

[33] J. Johnson, A. Alahi, and L. Fei-Fei. Perceptual losses for real-time style transfer and super-resolution. In *ECCV*, pages 694–711, 2016.

[34] Diederik P. K. and Jimmy B. Adam. A method for stochastic optimization. In *ICLR Conference Track Proceedings*, 2015.

[35] A. Keshavan, J. D. Yeatman, and A. Rokem. Combining Citizen Science and Deep Learning to Amplify Expertise in Neuroimaging. *Frontiers in Neuroinformatics*, 0:29, 2019.

[36] V. Khrulkov and I. V. Oseledets. Geometry score: A method for comparing generative adversarial networks. In *ICML*, volume 80 of *Proceedings of Machine Learning Research*, pages 2626–2634, 2018.

[37] Jayant Kumar, Peng Ye, and David Doermann. A Dataset for Quality Assessment of Camera Captured Document Images. *Lecture Notes in Computer Science*, 8357 LNCS:113–125, 2013.

[38] Eric Cooper Larson and Damon Michael Chandler. Most apparent distortion: full-reference image quality assessment and the role of strategy. *Journal of Electronic Imaging*, 19(1):011006, jan 2010.

[39] R. Li, G. Dai, Z. Wang, S. Yu, and Y. Xie. Using signal-to-noise ratio to connect the quality assessment of natural and medical images. In *ICDIP*, volume 10806, page 108064Q, 2018.

[40] Hanhe Lin, Vlad Hosu, and Dietmar Saupe. Kadid-10k: A large-scale artificially distorted iqa database. In *2019 Tenth Intern Conf on Quality of Multimedia Experience (QoMEX)*, pages 1–3. IEEE, 2019.

[41] R. A. Manap and L. Shao. Non-distortion-specific no-reference image quality assessment: A survey. *Information Sciences*, 301:141–160, 2015.

[42] A. Mittal, A. Krishna Moorthy, and A. C. Bovik. No-reference image quality assessment in the spatial domain. *IEEE Transactions on Image Processing*, 21(12):4695–4708, 2012.

[43] Pedram Mohammadi, Abbas Ebrahimi-Moghadam, and Shahram Shirianni. Subjective and objective quality assessment of image: A survey. *CoRR*, abs/1406.7799, 2014.

[44] Hossein Ziae Nafchi, Atena Shahkolaei, Rachid Hedjam, and Mohamed Cheriet. Mean deviation similarity index: Efficient and reliable full-reference image quality evaluator. *IEEE Access*, 4:5579–5590, 2016.

[45] Rafal Obuchowicz, Mariusz Oszust, Marzena Bielecka, Andrzej Bielecki, and Adam Piórkowski. Magnetic Resonance Image Quality Assessment by Using Non-Maximum Suppression and Entropy Analysis. *Entropy 2020, Vol. 22, Page 220*, 22(2):220, 2020.

[46] M. Oszust, A. Piórkowski, and R. Obuchowicz. No-reference image quality assessment of magnetic resonance images with high-boost filtering and local features. *MR in Medicine*, 84(3):1648–1660, 2020.

[47] Marius Pedersen. Evaluation of 60 full-reference image quality metrics on the CID:IQ. *Proceedings ICIP*, 2015-Decem:1588–1592, 2015.

[48] E. Prashnani, H. Cai, Y. Mostofi, and P. Sen. Pieapp: Perceptual image-error assessment through pairwise preference. In *2018 IEEE Conference on CVPR*, pages 1808–1817, 2018.

[49] Heshalini Rajagopal. Subjective versus Objective Assessment for Magnetic Resonance (MR) Images. In *17th International Conf on Communic and Inform Technology and Engineering*, volume 9, 2015.

[50] Artem Razumov, Oleg Y. Rogov, and Dmitry V. Dylov. Optimal MRI undersampling patterns for ultimate benefit of medical vision tasks. *CoRR*, abs/2108.04914, 2021.

[51] Rafael Reisenhofer, Sebastian Bosse, Gitta Kutyniok, and Thomas Wiegand. A haar wavelet-based perceptual similarity index for image quality assessment. *Signal Process. Image Commun.*, 61:33–43, 2018.

[52] G. P. Renieblas, A. T. Nogués, A. M. González, N. León, and E. G. del Castillo. Structural similarity index family for image quality assessment in radiological images. *Journal of Medical Imaging*, 4(3):035501, 2017.

[53] O. Ronneberger, P. Fischer, and T. Brox. U-net: Convolutional networks for biomedical image segmentation. In *MICCAI 2015 Proceedings, Part III*, volume 9351 of *Lecture Notes in CS*, pages 234–241, 2015.

[54] Tim Salimans, Ian Goodfellow, Wojciech Zaremba, Vicki Cheung, Alec Radford, and Xi Chen. Improved techniques for training gans. In *Adv Neural Inform Process Syst*, pages 2234–2242, 2016.

[55] H. R. Sheikh, M. F. Sabir, and A. C. Bovik. A statistical evaluation of recent full reference image quality assessment algorithms. *IEEE Transactions on Image Processing*, 15(11):3440–3451, 2006.

[56] Hamid R Sheikh and Alan C Bovik. A visual information fidelity approach to video quality assessment. In *The First International Workshop on Video Processing and Quality Metrics for Consumer Electronics*, volume 7, page 2. sn, 2005.

[57] V.R. Simi, Damodar Reddy Edla, and Justin Joseph. A no-reference metric to assess quality of denoising for Magnetic Resonance images. *Biomedical Signal Processing and Control*, 70:102962, 2021.

[58] K. Simonyan and A. Zisserman. Very deep convolutional networks for large-scale image recognition. In *ICLR*, 2015.

[59] K Sommer, A Saalbach, T Brosch, C Hall, NM Cross, and JB Andre. Correction of motion artifacts using a multiscale fully convolutional neural network. *American J. of Neuroradiology*, 41(3):416–423, 2020.

[60] I. Stępień, R. Obuchowicz, A. Piórkowski, and M. Oszust. Fusion of Deep Convolutional Neural Networks for No-Reference Magnetic Resonance Image Quality Assessment. *Sensors 2021, Vol. 21, Page 1043*, 21(4):1043, 2021.

[61] T. Tieleman and G. Hinton. Lecture 6.5-rmsprop, coursera: Neural networks for ML. *University of Toronto, Tech Report*, 2012.

[62] M. Tkachenko, M. Malyuk, N. Shevchenko, A. Holmanyuk, and N. Lubimov. Label Studio: Data labeling software, 2020. Open source software available from <https://github.com/heartexlabs/label-studio>, Online; Accessed on 3 March 2022.

[63] S Triantaphillidou, E Allen, and RE Jacobson. Image quality of jpeg vs jpeg 2000 image compression schemes, part 2: Scene analysis. *IS&T J. Imaging Sci. Technol*, 51(3):259–270, 2007.

[64] Anthony Viera and Joanne Garrett. Understanding interobserver agreement: The kappa statistic. *Family medicine*, 37:360–3, 06 2005.

[65] Eryan Wang, Bin Yang, and Lihui Pang. Superpixel-based Structural Similarity Metric for Image Fusion Quality Evaluation. *Sensing and Imaging 2021 22:1*, 22(1):1–25, 2021.

[66] Z. Wang. Applications of objective image quality assessment methods [applications corner]. *IEEE SPM*, 28(6):137–142, 2011.

[67] Z. Wang and A. C. Bovik. Modern image quality assessment. *Synthesis Lectures on Image, Video, and Multimedia Processing*, 2(1):1–156, 2006.

[68] Z. Wang, A. C. Bovik, H. R. Sheikh, and E. P. Simoncelli. Image quality assessment: from error visibility to structural similarity. *IEEE TIP*, 13(4):600–612, 2004.

[69] Z. Wang and Q. Li. Information content weighting for perceptual image quality assessment. *IEEE TIP*, 20(5):1185–1198, 2010.

[70] Z. Wang, E. P. Simoncelli, and A. C. Bovik. Multiscale structural similarity for image quality assessment. In *The 37th Asilomar Conference on Signals, Systems & Computers*, volume 2, pages 1398–1402, 2003.

[71] W. Xue, L. Zhang, X. Mou, and A. C. Bovik. Gradient magnitude similarity deviation: A highly efficient perceptual image quality index. *IEEE TIP*, 23(2):684–695, 2013.

[72] H. Yang, Y. Fang, and W. Lin. Perceptual Quality Assessment of Screen Content Images. *IEEE TIP*, 24(11):4408–4421, 2015.

[73] Z. Ying, H. Niu, P. Gupta, D. Mahajan, D. Ghadiyaram, and A. C. Bovik. From patches to pictures (paq-2-piq): Mapping the perceptual space of picture quality. In *2020 IEEE/CVF Conference CVPR*, pages 3572–3582, 2020.

[74] B. Zhang, P. V. Sander, and A. Bermak. Gradient magnitude similarity deviation on multiple scales for color image quality assessment. In *2017 IEEE ICASSP*, pages 1253–1257, 2017.

[75] L. Zhang, Y. Shen, and H. Li. VSI: A visual saliency-induced index for perceptual image quality assessment. *IEEE Transactions on Image processing*, 23(10):4270–4281, 2014.

[76] L. Zhang, L. Zhang, X. Mou, and D. Zhang. FSIM: A feature similarity index for image quality assessment. *IEEE TIP*, 20(8):2378–2386, 2011.

[77] L. Zhang, L. Zhang, X. Mou, and D. Zhang. A comprehensive evaluation of full reference image quality assessment algorithms. *Proceedings - ICIP*, pages 1477–1480, 2012.

[78] R. Zhang, P. Isola, A. A Efros, E. Shechtman, and O. Wang. The unreasonable effectiveness of deep features as a perceptual metric. In *Proceedings of the IEEE Conference CVPR*, pages 586–595, 2018.

[79] H. Zhu, L. Li, J. Wu, W. Dong, and G. Shi. Metaiqa: Deep meta-learning for no-reference image quality assessment. In *2020 IEEE/CVF Conference CVPR*, pages 14131–14140, 2020.